**Ocean Science
Discussions**

Comparing historical and modern methods of Sea Surface Temperature measurement – Part 2: Field comparison in the Central Tropical Pacific

J. B. R. Matthews[1] and J. B. Matthews[2]

[1]School of Earth and Ocean Sciences, University of Victoria, Victoria, BC, Canada
[2]Dr. J. B. Matthews Consulting, Tennis Road, Douglas, Isle of Man, British Isles

Correspondence to: J. B. R. Matthews (georobin@uvic.ca)

Title Page	
Abstract	Introduction
Conclusions	References
Tables	Figures

◄◄	►►
◄	►
Back	Close

Full Screen / Esc

Printer-friendly Version

Interactive Discussion

J. B. R. Matthews and
J. B. Matthews

Abstract

Discrepancies between historical Sea Surface Temperature (SST) datasets have been partly ascribed to use of different adjustments for variable measurement methods. Until recently adjustments had only been applied to bucket temperatures from the late 19th and early 20th century, with the aim of correcting their supposed coolness relative to engine cooling water intake temperatures (EIT). In the UK Met Office Hadley Centre SST 3 dataset (HadSST3) adjustments are applied to observations over its full duration, including those obtained by other methods. Here we evaluate such adjustments by direct field comparison of historical and modern methods of SST measurement.

We compare wood, canvas and rubber bucket temperatures to 3 m seawater intake temperature along a Central Tropical Pacific transect conducted in May and June 2008. In contrast to the prevailing view we find no average differences between bucket temperatures obtained with different bucket types. Moreover, we observe strong near-surface temperature gradients day and night, indicating intake and bucket temperatures cannot be considered equivalent in this region. We suggest engine intake temperatures are unreliable as a source of SST given that they are often obtained by untrained non-scientist observers with low precision, inaccurate instruments at unknown intake depth. Using a physical model we demonstrate that warming of intake seawater by engine room air is unlikely a cause of negative average bucket-intake temperature differences, as sometimes suggested. We propose removal of intake temperatures and bucket adjustments from historical SST records and posit this will lead to their better capture of real long-term trends.

1 Introduction

Here we address issues surrounding construction of Sea Surface Temperature (SST) datasets using observations obtained from a mix of different platforms, instruments and depths. Modern platforms include ships, moored and drifting buoys and satellites, with

Field comparison of SST measurement methods

J. B. R. Matthews and
J. B. Matthews

shipboard measurements mostly obtained from buckets, engine cooling water intakes and hull contact sensors. Measurement methods were reviewed in detail in Part 1.

Satellite-based methods measure temperature within the sea surface skin (upper $\sim 1\,mm$) whereas in situ methods measure the so-called bulk temperature beneath (Donlon et al., 2002). Skin temperatures are generally a few tenths of a °C colder than the bulk temperature immediately below. Here we distinguish between different types of bulk temperature based on sampling depth. We consider temperatures observed beneath the surface skin and within the upper 1 m as measurements of actual sea surface temperature. These are the depths typically sampled by buckets, drifting buoys and the uppermost thermometers on moored buoys. Temperatures obtained below 1 m and above 30 m are referred to as near-surface temperatures. These depths are sampled by seawater intakes, Conductivity-Temperature-Depth (CTD) casts and hull contact sensors. Near-surface temperatures of sufficient depth to be free of diurnal variability are referred to as foundation temperatures. As noted in Part 1, intake depths on modern merchant vessels are generally around 7–10 m, although can exceed 15 m.

Adjustments have been applied to several historical SST datasets in attempts to reduce supposed average offsets between different measurement methods. This can result in substantial alteration of long-term trends at both global and more localized scales. For instance, Vecchi et al. (2008) identify discrepancies between the Tropical Pacific records of two SST datasets and suggest they may partly result from different adjustments to bucket temperatures. They find the US National Oceanic and Atmospheric Administration's (NOAA) Extended Reconstruction SST version 2, ERSSTv2 (Smith and Reynolds, 2004) and UK Met Office Hadley Centre Sea Ice and SST, HadISST (Rayner et al., 2003) datasets exhibit different centennial trends in east-west SST gradients across the Tropical Pacific. Whilst HadISST shows a trend towards more La Niña-like conditions, ERSSTv2 trends towards more El Niño-like conditions. Comparing pre-1950 SST anomalies in the Niño-3.4 region (5° S–5° N, 120°–170° W) in HadISST and the third version of ERSST, ERSSTv3, Smith et al. (2008) found HadISST to be $\sim 0.3\,°C$ warmer, largely the result of different bucket adjustments prior to 1942.

Similar bucket adjustments as applied to HadISST have also been applied to the second and third versions of the Hadley Centre SST dataset, HadSST2 (Rayner et al., 2006) and HadSST3 (Kennedy et al., 2011a, b). All were based on those of Folland and Parker (1995, referred to as FP95), described in Part 1. Within the portion of the Central Tropical Pacific covered during the field comparison reported here, average bucket adjustments for 1910–1930 applied in HadSST2 are around +0.4–0.6 °C (Kent et al., 2010). Those applied to ERSSTv3, derived by Smith and Reynolds (2002), are smaller at around +0.1–0.4 °C.

Here we evaluate adjustments applied to SST datasets by field comparison of historical and modern methods of shipboard SST measurement. Section 2 describes the methodology of our field experiment. Analysis of results forms Sect. 3 and includes discussion of calculations to determine whether intake seawater could be warmed by engine room air prior to measurement. Conclusions, recommendations for future field studies and proposals for changes to historical SST datasets are outlined in Sect. 4.

2 Methodology

Original data were collected on a 5-week research cruise from Papeete, Tahiti to Honolulu, Hawaii aboard the *SSV Robert C. Seamans* from 9 May to 14 June 2008 (Siuda, 2008; Matthews, 2009). The *Seamans* is a ∼ 41 m-long modern sailing vessel of draft ∼ 4 m, achieving typical speeds of ∼ 2–6 kt (∼ 1–3 m s^{-1}) under-sail and ∼ 7–9 kt (∼ 3.5–4.5 m s^{-1}) under-motor. She would be considered a "slow" ship by the FP95 definition. The vessel is equipped with physical, chemical, biological and geological oceanographic sampling equipment and is a World Meteorological Organization (WMO) Voluntary Observing Ship (VOS), reporting once daily.

Several sea surface and near-surface temperature measurement methods were directly compared along the cruise transect (Fig. 1), which was conducted at the end of the 2007/8 La Niña. Hourly bucket temperatures were obtained from ∼ 17.5° S to ∼ 3° N using three different bucket types and various meteorological measurements recorded

Field comparison of SST measurement methods

J. B. R. Matthews and
J. B. Matthews

Title Page

Abstract | Introduction

Conclusions | References

Tables | Figures

◄ | ►

◄ | ►

Back | Close

Full Screen / Esc

Printer-friendly Version

Interactive Discussion

near-simultaneously. Subsurface thermosalinograph temperature at $\sim 3\,\mathrm{m}$ depth was measured each minute between 17.5° S and 19° N and considered analogous to accurate engine intake temperature (EIT) for the same intake depth. Daytime temperature profiles to 20 m were obtained by CTD at the locations marked in Fig. 1. This enabled assessment of temperature variation in the depth range of VOS intakes.

2.1 Bucket temperatures

Near-continuous hourly bucket temperatures were taken for 10 consecutive local days from May 11th to 20th 2008 between 17.09° S, 149.77° W and 8.95° S, 140.30° W. Measurements then temporarily ceased for a port call at Nuku Hiva in the Marquesas Islands. Daily-average track coverage during this period was 80 ± 21 nautical miles ($149 \pm 38\,\mathrm{km}$), $0.8 \pm 0.2°$ latitude and $0.9 \pm 0.6°$ longitude. Bucket measurements resumed for the first full local day on 25 May at 8.83° S, 140.35° W and continued until 3.08° N, 143.23° W on the morning of 1 June.

Bucket temperatures were obtained using wood, canvas and a modern rubber meteorological bucket (Zubrycki bucket) in what was apparently the first field comparison of wood and canvas bucket temperatures. The wood and canvas buckets were of similar size (wood: 22.5 cm inner diameter by 18 cm high, volumetric capacity $\sim 0.007\,\mathrm{m}^3$; canvas: 24 cm by 26 cm, capacity $\sim 0.011\,\mathrm{m}^3$; Fig. 2), with the canvas bucket being a modern general-purpose ships' bucket. The wood bucket is of similar diameter but reduced height to the 19th century wooden ships' bucket modelled by FP95 (25 cm inner diameter by 25 cm high, volumetric capacity $\sim 0.012\,\mathrm{m}^3$). Whilst constructed of softwood pine rather than the hardwood oak of the FP95 wood bucket, pine is of similar specific heat capacity to oak ($\sim 2.5\,\mathrm{kJ\,kg}^{-1}\,\mathrm{K}^{-1}$ compared to $\sim 1.9\,\mathrm{kJ\,kg}^{-1}\,\mathrm{K}^{-1}$). The volumetric capacity of our canvas bucket is nearly three times that described by Brooks (1926) ($\sim 0.004\,\mathrm{m}^3$; 5 inches ($\sim 13\,\mathrm{cm}$) diameter by 14 inches ($\sim 36\,\mathrm{cm}$) high) and that of the UK Met Office Mk II canvas meteorological bucket ($\sim 0.004\,\mathrm{m}^3$, 16 cm by 25 cm, fillable to $\sim 20\,\mathrm{cm}$ deep). However, it is of similar capacity to canvas buckets used by Japanese ships around the 1930 s (~ 0.012–$0.028\,\mathrm{m}^3$, 20–30 cm diameter by

Field comparison of SST measurement methods

J. B. R. Matthews and
J. B. Matthews

40 cm high; Uwai and Komura, 1992). Unlike the Mk II our canvas bucket did not have a wooden lid or base and could be placed on deck without collapse. Our rubber bucket had the smallest volumetric capacity at $\sim 0.0007\,\mathrm{m}^3$ (7.5 cm inner diameter by 16.5 cm high), smaller than the 5 l ($0.005\,\mathrm{m}^3$) rubber bucket used by Tabata (1978). A transparent plastic tube extends from the base to house a thermometer, although one was not fitted. Temperatures from this bucket were used as our reference, with captured seawater samples assumed not to warm or cool prior to measurement.

Bucket temperatures were collected underway by 18 undergraduate students (a mixture of Science and Arts majors) working on a three-watch system. This simulates multiple observers in historical datasets. At each bucket station the three buckets were consecutively cast overboard, filled with seawater, hauled up and placed on the wooden deck. A new factory-calibrated Fisher traceable thermistor probe with 0.1 °C resolution was inserted into each bucket sample and a reading recorded once the display stabilised in around 10–20 s. Stations were within five minutes prior to the top of a given hour. Deployment, retrieval and measurement were conducted on the port side outside the wet lab, a location that frequently switched from leeward to windward. The buckets were not deliberately placed in the shade or a wind-exposed location for measurement but were stored in the wet lab between stations. The walls of the wood and canvas buckets generally remained wet between measurements. Hauling times were short given that bucket launch and retrieval was from $\sim 2.5\,\mathrm{m}$ above the waterline. The total hauling and on-deck measurement period ("exposure time") was $\sim 1\,\mathrm{min}$.

Sampling was easiest with the rubber bucket since this would dip near-vertically into the sea surface and so did not need to be dragged to obtain a sample like the wood and canvas buckets. The canvas bucket tended to close flat when dragged and not fill while the wood bucket would bounce along the sea surface when under-motor. Several attempts were sometimes required to capture sufficient samples with the wood and canvas buckets (around two-thirds capacity) whereas the rubber bucket would consistently fill to the brim. Retrieval of the wood and canvas buckets became difficult if too much line was released and they drifted far back towards the stern.

2.2 Meteorological observations

Several meteorological variables were recorded near-contemporaneously with each bucket station. Dry and wet bulb air temperatures were taken from liquid-in-glass thermometers mounted in a Stevenson screen on the poop deck ($\sim 5\,\mathrm{m}$ above the waterline). Given a typical tropospheric lapse rate of $\sim 6.5 \times 10^{-3}\,^\circ\mathrm{C}\,\mathrm{m}^{-1}$, the difference between air temperature immediately above the sea surface and at this measurement height would be $< 0.05\,^\circ\mathrm{C}$, far below the precision to which the dry and wet bulb thermometers were read (0.5 or $1\,^\circ\mathrm{C}$). Beaufort wind force and cloud cover in oktas were estimated by eye and atmospheric pressure read from a barometer installed in the deckhouse.

Wind speed and direction were measured each minute by anemometer atop the foremast at $\sim 33\,\mathrm{m}$ above the waterline. True wind speed at 33 m (U_{33}) was converted to wind speed at other heights (U_z) using the log-profile formula from the TurboWin software, reported in Thomas et al. (2005) as:

$$U_z = U_{33} \frac{\ln\left(\frac{z}{0.0016}\right)}{\ln\left(\frac{33}{0.0016}\right)} \tag{1}$$

TurboWin is a meteorological logbook program widely used by the European VOS (Kent et al., 2007). Wind speed and direction from $\leq 5\,\mathrm{min}$ prior to the top of each hour were averaged for comparison to hourly measurements.

2.3 Subsurface measurements

Scientific seawater intake temperature was recorded at 1 min intervals by thermosalinograph or TSG (Seabird SBE45, accurate to at least $0.01\,^\circ\mathrm{C}$) from 17.5° S to 19° N. The TSG measures seawater in the scientific flow-through, sampled by a sea chest at $\sim 3\,\mathrm{m}$ depth and piped up to the TSG in the wet lab at the main external deck level. In the absence of an engine cooling water intake on the *Seamans*, TSG temperature was used

Title Page

Abstract | Introduction

Conclusions | References

Tables | Figures

◄ | ►|

◄ | ►

Back | Close

Full Screen / Esc

Printer-friendly Version

Interactive Discussion

as an analogue for accurate EIT at the same sampling depth. TSG temperature was averaged as per wind speed and direction for comparison to hourly measurements.

CTD casts with a Seabird SEACAT Profiler (SBE19plus, temperature accurate to at least 0.01 °C) were taken hove-to at 22 locations along the transect (Fig. 1). Mean speed over ground whilst hove-to was 1.4 ± 0.7 kt ($\sim 0.7 \pm 0.4$ m s^{-1}), with hove-to periods identified from coincident changes in apparent wind direction. At each location, CTD temperature was recorded every 5 m at nominal depths between 5 and 20 m. Besides two mid-afternoon casts observed around 15:30–16:30 LT (local time) (CTD-1 and CTD-22), all casts were taken in mid to late morning between 09:00 a.m. and noon. Note that local time was UTC minus 10 h. Eastward surface current velocity at ~ 19 m depth was measured every 20 min using a shipboard Acoustic Doppler Current Profiler or ADCP (RDI Ocean Surveyor 75 kHz).

2.4   OSTIA data

Daily foundation temperatures from the Operational Sea Surface Temperature and Sea Ice Analysis (OSTIA) were obtained for comparison to our shipboard temperatures. OSTIA is a high resolution (1/20°, ~ 6 km) gridded dataset derived from buoy, ship and satellite (infrared and microwave) observations by optimal interpolation (Donlon et al., 2012). Temperatures obtained in daytime under low wind speeds (< 6 m s^{-1}) are rejected in an attempt to exclude measurements influenced by formation of a diurnal thermocline.

OSTIA is used as a boundary condition for weather forecast models at the UK Met Office and European Centre for Medium-range Weather Forecasting. Note that the equatorial Pacific can be a problematic region for SST measurement by satellite-mounted infrared sensors due to the thick band of cumulonimbus clouds associated with the Intertropical Convergence Zone and high relative humidities (generally $> 70\%$ along our transect).

The OSTIA system uses a rolling 36 h observation window centered on 12:00 UTC with a single field produced for each UTC day. OSTIA grid cells traversed by the *Seamans* on each local day were identified and corresponding foundation temperatures extracted and averaged for the equivalent OSTIA UTC day. Difference in phasing of local and UTC days was ignored given the long observation window.

3 Results and discussion

3.1 Bucket temperature comparison

Little difference was found between wood, canvas and rubber bucket temperatures, with mean differences of $0.0 \pm 0.1\,°C$ between all bucket types (Fig. 3). This was also the case when observations were separated by day and night, with daytime measurements taken to be those obtained between the local times of sunrise and sunset and vice versa for nighttime measurements. When partitioned into the regions identified in Table 1 and Fig. 4, absolute mean inter-bucket temperature differences were under $0.1\,°C$, with standard deviations around $±0.1$ to $±0.2\,°C$. This was also true when observations were further separated by day and night, except for daytime measurements from the North Equatorial Countercurrrent (NECC) outside the equatorial cold tongue where sample size was < 10. Some of the non-zero temperature differences may be due to misreading of the thermistor display and/or recording error. The largest reported difference was $0.7\,°C$ between rubber and canvas bucket temperatures at one station (excluded from Fig. 3b).

An unintended experiment occurred after the wooden bucket was damaged $\sim 9°$ S, leaking heavily thereafter. No evidence was found that this had any effect on measured temperatures (i.e. there was no change in the mean or standard deviation of wood-canvas or rubber-wood bucket temperature differences) despite the seawater samples draining completely in a few minutes. Leaking wooden bucket temperatures were thus retained for all analyses.

Field comparison of SST measurement methods

J. B. R. Matthews and J. B. Matthews

Title Page

Abstract	Introduction
Conclusions	References
Tables	Figures

| ◄◄ | ►► |
| ◄ | ► |

Back | Close

Full Screen / Esc

Printer-friendly Version

Interactive Discussion

The rubber bucket temperatures show a slight cool tendency relative to those from the canvas and wood buckets, with rubber-canvas and rubber-wood differences of −0.1 °C found for a relatively large number of stations (26 and 30 %, respectively). This might reflect a slight susceptibility for the rubber bucket samples to cool prior to measurement due to their smaller volume. Even so, assumption that the rubber bucket seawater samples remain of stable temperature prior to measurement is a reasonable approximation. We conclude our bucket temperatures are accurate to 0.1 °C and average over temperatures from different bucket types at each station to create a "composite" bucket temperature variable.

No correlations were found between inter-bucket temperature differences and apparent wind speed at 3 m, apparent wind direction, ship speed over ground, local time, atmospheric pressure, air minus composite bucket temperature difference or relative humidity. To assess correlations between inter-bucket differences and meteorological variables estimated by eye (i.e. Beaufort wind force and cloud cover), temperature differences were split into two groups from coincidence with high or low values of these meteorological variables. High wind forces were considered those ≥ 4 and high cloud cover ≥ 5 oktas. All groupings were found to have means of 0.0 ± 0.1 °C, so again there were no correlations.

Our results suggest accurate bucket temperatures can be obtained by rapid hauling and measurement using fast-response scientific thermometers and buckets of large volumetric capacity. We find no evidence for evaporative cooling of seawater samples in our wood and canvas buckets in the ∼ 1 min exposure period.

Our results are markedly different from the strong cooling rates computed by FP95. Their bucket adjustments for the Tropical Pacific are amongst the largest derived on an annual-average due to their calculated strong and seasonally-invariant evaporation rates. Their final adjustments for June in the Central Tropical Pacific are around 0.1–0.3 °C and 0.4–0.7 °C in 1860 and 1940, respectively. The corresponding adjustments for December are around 0.1–0.2 °C and 0.4–0.6 °C. These values are not directly comparable to our results given the longer exposure times used by FP95 (4 min for the

wooden bucket adjustments) and our different bucket sample volumes. At two-thirds full our canvas bucket contained around twice the filled volume of the Mk II ($\sim$ 0.008 to $\sim$ 0.004 m^3), the larger of the two canvas buckets modelled by FP95. Conversely the modelled volume in their wooden bucket (water depth 20 cm) was around twice that of ours at two-thirds capacity ($\sim$ 0.010 to $\sim$ 0.005 m^3).

These may not be the only reasons for the discrepancy between our results and those of FP95. Critically their canvas bucket model assumes the seawater sample well-mixed and at the same temperature as the bucket walls. We question this assumption given that seawater does not convect as freely as freshwater and bucket samples are unlikely to have been actively stirred. Thus evaporative cooling could be restricted to the seawater immediately adjacent to the canvas walls with the resultant heat loss not measurable by a thermometer bulb in the sample interior.

3.2 Vertical near-surface temperature gradients

Given that our bucket temperatures appear accurate, they can be used together with subsurface temperatures from the TSG and CTD casts to reveal near-surface temperature gradients within the depth range of VOS intakes. Here we restrict discussion to vertical gradients within the coverage of the bucket measurements ($\sim$ 17.5° S to $\sim$ 3° N). Strong gradients were observed day and night throughout this portion of the transect (Fig. 5, Table 1), with the average temperature difference over the upper 3 m being $-0.4 \pm 0.2\,^\circ$C. Nighttime gradients were weaker than daytime gradients over the upper 3 m at $-0.10\,^\circ$C m^{-1} compared to $-0.16\,^\circ$C m^{-1}, with the corresponding average upper 3 m differences being $-0.3 \pm 0.1\,^\circ$C and $-0.5 \pm 0.2\,^\circ$C. Evidently the near-surface thermocline did not breakdown overnight, in contrast to observed behaviour in the Western Equatorial Pacific (Soloviev and Lukas, 2006). Differences across the upper 3 m were found to be strongest in early to mid-afternoon (around 12:00–15:00 LT) and weakest overnight from 19:00–07:00 LT (Fig. 6). This is a consequence of diurnal temperature cycles being of larger amplitude at the surface than at 3 m. Diurnal air temperature cycles were larger still due to the lower specific heat capacity of air. Diurnal ranges in

composite bucket SST were large in the weak and moderate branches of the South Equatorial Current (SEC) averaging $0.9 \pm 0.3\,^{\circ}$C and somewhat reduced in its strong branch averaging $0.6 \pm 0.1\,^{\circ}$C. The corresponding average diurnal ranges in 3 m TSG temperature were $0.5 \pm 0.2\,^{\circ}$C and $0.3 \pm 0.1\,^{\circ}$C.

Thermoclines were found across the upper 5–15 m in all CTD casts (Fig. 7), with temperature differences and gradients over the upper 5 m respectively averaging $-0.8 \pm 0.2\,^{\circ}$C and $-0.16\,^{\circ}$C m^{-1} for morning casts. Gradients between 5 and 10 m were generally weak with temperature differences averaging $-0.08 \pm 0.08\,^{\circ}$C over morning casts, although several differences around -0.1 to $-0.3\,^{\circ}$C were found. Temperature declines between 10 and 15 m ranged from 0.00–$0.03\,^{\circ}$C in the same casts. The only afternoon cast with a corresponding composite bucket temperature, CTD-1, recorded temperatures $1.3\,^{\circ}$C colder at 10 m than at the surface, with the coincident gradient across the upper 5 m being around $-0.24\,^{\circ}$C m^{-1}. Temperature differences between 5 and 10 m, and 10 and 15 m were -0.11 and $-0.07\,^{\circ}$C, respectively. The temperature difference over the upper 3 m was $-0.9\,^{\circ}$C, close to the largest observed, which was around $-1\,^{\circ}$C. Strong near-surface temperature gradients like these are thought ubiquitous under weak winds and strong insolation.

Interestingly the near-surface thermocline persisted when 10 m wind speeds exceeded 6 m s^{-1} (Fig. 8a), both day and night, in contrast to general thinking (Soloviev and Lukas, 2006; Donlon et al., 2012). Daytime upper 3 m temperature differences exceeding $0.7\,^{\circ}$C were, however, generally not encountered under these conditions. Note that where 10 m wind speeds exceeded 6 m s^{-1}, all remained below 10 m s^{-1} except in one case.

We find no correlation between upper 3 m temperature differences and ship speed over ground (Fig. 8b), suggesting measured near-surface temperature gradients were not disturbed by ship motion. As a further test we compared average 3 m TSG temperatures for periods when the ship was hove-to for scientific sampling with those for the 30 min periods immediately before and after. A mean difference of $0.0 \pm 0.1\,^{\circ}$C was found, again suggesting ship motion did not strongly mix the near-surface.

Title Page

Abstract | Introduction

Conclusions | References

Tables | Figures

◄◄ | ►►

◄ | ►

Back | Close

Full Screen / Esc

Printer-friendly Version

Interactive Discussion

3.3 Comparison to OSTIA

Foundation temperatures from OSTIA are comparable to our CTD temperatures at 15 m (Fig. 5b), the depth at which we consider near-surface temperatures free of diurnal variability. The CTD_{15m}-OSTIA temperature difference from all CTD casts averaged 0.0±0.2 °C, smaller than the supplied OSTIA errors which ranged from ±0.3 to ±0.8 °C. The OSTIA temperatures successfully capture daily-average near-surface meridional gradients, although with only a limited number of CTD casts for comparison in the North Equatorial Current (NEC). A temperature dip observed in daily-average composite bucket SST in the moderate branch of the South Equatorial Current is particularly pronounced in OSTIA, with temperatures dropping $\sim$ 0.8 °C from the weak SEC regime. OSTIA temperatures were closest to daily-average 3 m temperatures in the NECC outside the cold tongue but were still $\sim$ 0.2 °C cooler. Evidently it would be inappropriate to substitute OSTIA foundation temperatures for daily-average bucket SST.

3.4 Intake temperature errors and engine room warming

Where EIT have been found to average warmer than bucket temperatures, heating of intake seawater by warm engine room air has often been suggested as a potential cause (e.g. Saur, 1963). To test this idea we developed a physical model for warming of intake seawater by net heat transfer into the intake pipe across the pipe wall. Our model is based on standard calculations from chemical engineering (McCabe et al., 2001). Fixed parameters were set so as to maximise computed seawater warming. Pipe wall thickness was varied in tandem with outside diameter (o.d.) according to Table A1, with the largest common wall thickness used for each standard outside diameter. Note that real engine intake pipes are of lower schedule than those modelled. Flow velocity and engine room air temperature were held fixed at lower and upper limits of $1\,\mathrm{m\,s^{-1}}$ and 50 °C, respectively. The model is derived in Appendix A.

Calculated warming after a 20 m length of pipe (an upper limit for inlet-thermometer distance) with variable o.d. and inlet temperature is presented in Fig. A3. Warming

is enhanced with larger temperature contrast across the pipe wall (i.e. as inlet temperature is lowered). Calculated warming is minimal for all but the smallest o.d. pipes and largest temperature contrasts. Engine intakes on merchant vessels generally have outside diameters exceeding 20 cm (discussed in Appendix A), for which computed warming was below 0.05 °C. Thus heating of intake seawater by engine room air is unlikely a major cause of reported negative average bucket-intake temperature offsets of several tenths of a °C.

This was previously noted by James and Shank (1964) who found that given an 8-inch (~ 20 cm) diameter pipe, a 2000 gallon min^{-1} (~ 3.8 m s^{-1}) flow rate and a 30 °F (~ 16.5 °C) temperature difference across the pipe wall, over 1000 ft (~ 305 m) of pipe would be required for a 0.1° F (~ 0.05 °C) temperature rise. Modelling a standard 21.91 cm o.d. pipe with 20.63 cm inside diameter (schedule 20) and flow velocity of upper limit (3 m s^{-1}) with this temperature contrast, we find a 0.1° F temperature rise would require a pipe length ~ 432 m. Pipe lengths necessary to achieve along-pipe warming of 0.2 °C are plotted in Fig. A4, again for a range of outside diameters and temperature contrasts. The minimum pipe length required is ~ 92 m for o.d. above 20 cm and the longest ~ 737 m. These are far greater than the inlet-thermometer distances reported in the literature (Table A2).

Other explanations for warm bias in intake temperatures besides engine room warming include heating of thermometers by conduction along metal fittings (Saur, 1963) and gradual warming of stagnant intake seawater around pumps (Brooks, 1926) or in faucet pipes (Piip, 1974) by engine room air. Intake temperatures from ice class vessels traversing high latitudes may be influenced by mixing of exhaust intake with fresh intake prior to use as a cooling agent, a process designed to prevent engine shock. It is unclear whether this is the case for any intake temperatures in the International Comprehensive Atmosphere-Ocean Data Set, ICOADS (Woodruff et al., 2011), the primary compilation of historical SST measurements.

Suggestion of physical causes for average EIT errors is, however, generally inappropriate given the noise in the observations. Variability in EIT measurements likely

reflects poor observation and recording. Poor quality is unsuprising given that these measurements were traditionally obtained by ships' engineers for engine monitoring purposes, where accuracy of 1–2 °C is sufficient. Sailors are likely to record to at most the smallest graduation on the thermometer used, which as noted in Part 1, appears often to have been around 1 °C or °F for intake thermometers. A preference for whole-number values was indeed found in our dry bulb air temperature measurements where the thermometer was marked in 1 °C intervals. Intake thermometers have also sometimes been noted as difficult to read, with unclear graduations and locations close to floor level (Brooks, 1926). They may be particularly prone to drift in the harsh engine room environment are often poorly-calibrated even today.

4   Conclusions and recommendations

Progress in the field of historical SST reconstruction has been hampered by neglect of near-surface dynamics, lack of direct field comparisons between measurement methods, limited metadata and observations of variable quality. We find no evidence for cold bias in wood or canvas bucket temperatures in the Central Tropical Pacific when measurement is rapid and buckets of large volume. Our results suggest susceptibility of bucket samples to heat loss or gain is likely more dependent on their volume than bucket material. We suggest volumetric capacity be the primary consideration in design of meteorological buckets. Additional field experiments should test whether our findings apply in other seasons and ENSO conditions and to historically-used buckets of smaller volume and different type. Experiments should be conducted on vessels of different class and in other ocean regions. In particular, accuracy of bucket temperatures from modern merchant vessels should be tested, on which hauling times would be longer and apparent wind speeds stronger. Studies could initially target those regions and seasons where bucket cooling is predicted to be largest (e.g. the Gulf Stream in winter). Field experiments with buckets would benefit from continuous monitoring of bucket sample temperature during the hauling and on-deck phase. This could be

achieved by attachment of a rugged electronic thermometer and datalogger to the bucket wall. This would also yield estimates of hauling time, apparently unreported since Brooks (1926). Combined with estimates of equilibration time for a range of fast and slow-response liquid-in-glass thermometers used historically, exposure time could thus be better constrained.

While the results of our bucket comparison are not directly comparable to the adjustments of FP95, we question their derivation and use of long sample exposure times (4 min for wooden buckets). As described in Part 1, they derived canvas bucket exposure times using their finding that seasonal SST cycles in the extratropics are of generally larger amplitude prior to 1942. Although not stated directly, their method effectively assumes seasonal cycles of spatially co-located bucket and intake temperatures should be the same in their 1951–1980 reference period. However, if seasonal cycles in the extratropics are, in fact, generally larger at the surface compared to, say, 5–10 m depth, then the larger amplitude cycles of pre-1942 years could be attributed to sampling being from a generally shallower depth (more bucket than intake observations). Regional synthesis of climatological seasonal temperature cycle amplitudes at various depths in the near-surface would be required to test this alternative explanation (e.g. using moored buoy data).

Given our observed lack of bucket cooling and the likelihood that exposure periods were far shorter than previously assumed (as discussed in Part 1), the very large bucket adjustments of FP95 (up to 0.7 °C in the Central Tropical Pacific) seem unrealistic. Critically we posit that any data of such poor quality that "correction" by application of such large, uncertain and complex adjustments becomes necessary should not be in scientific usage. Whilst historical bucket temperatures appear to have been of reasonable accuracy, we suggest engine intake temperatures unreliable for climate research. Bucket temperatures seem to have typically been observed with dedicated instruments by deck crew experienced in weather observation. Engine intake temperatures, on the other hand, have traditionally been taken by ships' engineers for engine monitoring purposes, where accuracy of only 1–2 °C is required. Intakes also sample at variable

and often unknown depth. Intake depths have been reported for some VOS ships since 1995 but remain unknown in many cases and are assumed invariant even where they are reported. Thus EIT generally cannot be corrected for near-surface temperature gradients even if these were known. Near-surface gradients are particularly strong in the Central Tropical Pacific where we found daytime temperature differences of up to 1.3 °C between the surface and 10 m. Our average upper 3 m temperature difference between ∼ 17.5° S and ∼ 3° N was −0.4 ± 0.2 °C, with such strong gradients persisting even when 10 m wind speeds exceeded 6 m s^{-1}.

The extent to which mechanical stirring by VOS ship propellers and motion acts to disturb near-surface temperature gradients is unclear, as is its influence on measured bucket and intake temperatures. The latter likely depends on sampling point, with the near-surface probably less disturbed away from the stern. Evidently findings of large negative average bucket-intake temperature offsets cannot reflect typical near-surface temperature gradients. Our physical modelling suggests they are also not likely due to warming of intake seawater by engine room air.

We propose exclusion of engine intake and other subsurface (below 1 m depth) temperatures from historical SST records. Removal of subsurface temperatures will suppress artificial signals from variable measurement depth since the remaining in situ methods (bucket and buoy) measure at a more consistent and historically-invariant depth. Loss of spatial and temporal coverage due to exclusion of subsurface temperatures requires detailed consideration, but may not be as dramatic as first suspected. Post-World War II, bucket temperatures generally comprised at least 40–60 % of monthly shipboard observations until the introduction of moored and drifting buoys in the 1970s (Kennedy et al., 2011b). Note that around 2.5–15 % or more of monthly observations were of unknown method during this period. Improved metadata will thus be required to more completely identify measurements for exclusion. Historical meteorological data recovery initiates (e.g. Wilkinson et al., 2011) should target digitisation of bucket temperatures over intake temperatures from unknown depth.

Subsurface VOS temperatures could still contribute to knowledge of diurnal and seasonal near-surface hydrodynamics where accurate and of known sampling depth. Thermometers used for VOS measurements should ideally be calibrated before every cruise. Further, Sea Surface Salinity (SSS) should be considered of equal climatic importance to SST, yet is only measured on select VOS ships and not included in ICOADS. The Global Surface Underway Data project (Petit de la Villéon et al., 2010) is working to collate SSS measurements from VOS ships such as those obtained through the French SSS Observation Service (Delcroix et al., 2010). Reprogramming of Argo floats to measure temperature and salinity every meter in the upper 20 m would improve coverage of near-surface variability, particularly beyond the shipping lanes to which VOS are largely restricted. Synthesis of near-surface hydrodynamics from existing floats measuring at least two temperatures and/or salinities within the upper 10 m should also be conducted. Further data could be obtained by mounting additional thermometers on moored buoys in the upper 20 m.

Appendix A

Engine intake warming model

We developed the following model for heating of seawater flowing through a pipe to test whether engine room warming of intake seawater is physically plausible. Fixed-value model parameters are given in Table A3 together with their symbols, units and prescribed value(s) used to generate Figs. A3 and A4. Computed model variables and their symbols, units and range of values calculated in generation of Fig. A3 are given in Table A4. Illustrative schematics highlighting some of the basic model parameters and variables are provided in Figs. A1 and A2.

Volumetric flow rate through a pipe is given by:

$$\dot{v} = \frac{1}{\rho}\frac{\mathrm{d}m}{\mathrm{d}t} = \frac{1}{\rho}\dot{m} \tag{A1}$$

where ρ is density, m is mass, t is time and $\dot{m}$ the mass flow rate.

Flow velocity is given by:

$$u = \frac{\dot{v}}{A_c} \tag{A2}$$

where A_c is the inside cross-sectional area of the pipe.

For a cylindrical pipe of inside diameter D_i, $A_c = \frac{\pi D_i^2}{4}$. Outside diameter D_o is related to inside diameter through wall thickness, Δx by: $D_o = D_i + 2\Delta x$.

For a pipe of length L, the surface area of the inside wall is given by:

$$A_i = \pi D_i L \tag{A3}$$

Similarly the surface area of the outside wall, $A_o = \pi D_o L$.

A single heat transfer process is assumed to occur in each medium; free (natural) convection in the engine room air, conduction across the pipe wall and forced convection in the intake seawater. Radiative transfer is neglected.

From Fourier's Law of Conduction, rate of conductive heat transfer in one dimension is given by:

$$q_{\text{cond}} = kA\frac{\Delta T}{\Delta x} \tag{A4}$$

where ΔT is a positive temperature difference across a material of thermal conductivity k, surface area A and thickness Δx.

From Newton's Law of Cooling, the rate of convective heat transfer is given by:

$$q_{\text{conv}} = hA\Delta T \tag{A5}$$

Field comparison of SST measurement methods

J. B. R. Matthews and J. B. Matthews

Title Page

Abstract	Introduction
Conclusions	References
Tables	Figures

◄◄   ►►

◄   ►

Back   Close

Full Screen / Esc

Printer-friendly Version

Interactive Discussion

where h is the convective heat transfer coefficient. Since the surface area of a cylindrical pipe is different for the inside and outside walls, we replace A in Eq. (A5) with a log-mean cross-sectional area, $A_{lm} = \frac{\pi(D_o - D_i)}{\ln(\frac{D_o}{D_i})} L$.

Thin boundary layers or films exist along the inside and outside walls of intake pipes, with flow velocity reduced towards the wall and strong temperature gradients also present (Fig. A2). We define convective heat transfer coefficients for these inside and outside films, h_{if} and h_{of}, respectively.

Equating convective heat flow across the outside and inside films with conductive heat flow across the pipe wall we have:

$$q = h_{of}A_o(T_1 - T_2) = k_w A_{lm} \frac{T_2 - T_3}{\Delta x_w} = h_{if}A_i(T_3 - T_4) \tag{A6}$$

where T_{1-4} are defined as in Fig. A2, k_w is the thermal conductivity of the wall and Δx_w the wall thickness. We model an unlagged steel pipe.

Rearranging for the temperature contrasts driving the convective and conductive heat flow:

$$T_1 - T_2 = \frac{q}{h_{of}A_o} \tag{A7}$$

$$T_2 - T_3 = \frac{q\Delta x_w}{k_w A_{lm}} \tag{A8}$$

$$T_3 - T_4 = \frac{q}{h_{if}A_i} \tag{A9}$$

Title Page

Abstract | Introduction

Conclusions | References

Tables | Figures

|◄ | ►|

◄ | ►

Back | Close

Full Screen / Esc

Printer-friendly Version

Interactive Discussion

Combining Eqs. (A7), (A8) and (A9) we can solve for the outside and inside wall temperatures, T_2 and T_3 as:

$$T_2 = T_4 + \frac{\frac{\Delta x_w}{k_w A_{lm}} + \frac{1}{h_{if} A_i}}{\frac{1}{h_{of} A_o} + \frac{\Delta x_w}{k_w A_{lm}} + \frac{1}{h_{if} A_i}}(T_1 - T_4) \tag{A10}$$

$$T_3 = T_1 - \frac{\frac{\Delta x_w}{k_w A_{lm}} + \frac{1}{h_{of} A_o}}{\frac{1}{h_{of} A_o} + \frac{\Delta x_w}{k_w A_{lm}} + \frac{1}{h_{if} A_i}}(T_1 - T_4) \tag{A11}$$

Given that seawater temperature varies along the pipe, we replace T_4 with an average seawater temperature, $T_{ave} = \frac{T_{in} + T_{out}}{2}$ and $T_1 - T_4$ with a log-mean temperature difference, $\Delta T_{lm} = \frac{(T_1 - T_{in}) - (T_1 - T_{out})}{\ln(\frac{T_1 - T_{in}}{T_1 - T_{out}})}$. T_{in} and T_{out} are the seawater temperatures at the inlet and after pipe length L, respectively.

We can now define an overall inside heat transfer coefficient, U_i such that:

$$q = U_i A_i \Delta T_{lm} \tag{A12}$$

Summing Eqs. (A7), (A8) and (A9) and taking $T_1 - T_4 = \Delta T_{lm}$:

$$\Delta T_{lm} = q\left(\frac{1}{h_{of} A_o} + \frac{\Delta x_w}{k_w A_{lm}} + \frac{1}{h_{if} A_i}\right) \tag{A13}$$

We can now solve for U_i using Eq. (A12):

$$U_i = \frac{1}{\frac{A_i}{h_{of} A_o} + \frac{A_i \Delta x_w}{k_w A_{lm}} + \frac{1}{h_{if}}} \tag{A14}$$

The specific heat capacity of the intake seawater, c_p is related to its warming by:

$$q = \dot{m} c_p (T_{out} - T_{in}) \tag{A15}$$

Title Page

Abstract | Introduction

Conclusions | References

Tables | Figures

|◄ | ►|

◄ | ►

Back | Close

Full Screen / Esc

Printer-friendly Version

Interactive Discussion

Equating Eqs. (A12) and (A15) and substituting in Eq. (A3):

$$\dot{m}c_p(T_{out} - T_{in}) = U_i(\pi D_i L)\Delta T_{lm} \tag{A16}$$

Rearranging for the temperature change after pipe length L:

$$T_{out} - T_{in} = \frac{U_i(\pi D_i L)\Delta T_{lm}}{\dot{m}c_p} \tag{A17}$$

For the range of inside diameters adopted (Table A1) and our specified flow velocity of $1\,\mathrm{m\,s^{-1}}$, pipe flow is turbulent with Reynolds number, Re, exceeding 10 000. Note Reynolds number is calculated as: $Re = \frac{4\dot{m}}{\pi D_i \mu}$ with μ the dynamic viscosity.

We model convective heat transfer about the inside film (if) as for fully developed turbulent flow, using the empirical correlation of Gnielinski (1976) for a smooth tube:

$$Nu = \frac{\frac{f}{8}(Re - 1000)Pr}{1 + 12.7(\frac{f}{8})^{\frac{1}{2}}(Pr^{\frac{2}{3}} - 1)} \tag{A18}$$

where Nu is the Nusselt number, f the friction factor and Pr the Prandtl number given by $Pr = \frac{c_p \mu}{k}$.

Equation (A18) is valid for $0.5 < Pr < 2000$ and $3000 < Re < 5 \times 10^6$. We compute the friction factor using the explicit relation of Petukhov (1970): $f = (0.79\ln(Re) - 1.64)^{-2}$.

The convective heat transfer coefficient for the inside film is calculated as:

$$h_{if} = \frac{Nu_{if}k_{if}}{D_i} \tag{A19}$$

For convection about the outside film (of) we use the Nusselt number formulation of Tahavvor and Yaghoubi (2008) for natural convection around a cold horizontal cylinder:

$$Nu_{of} = 0.3607 R_{aD}^{0.2802} \tag{A20}$$

where R_{aD} is the Rayleigh number based on D_o as the characteristic length and given by: $R_{aD} = \frac{g\beta_{of}}{\alpha_{of}\nu_{of}}(T_1 - T_2)D_o^3$ (Homayoni and Yaghoubi, 2008). β_{of} is the thermal expansion coefficient, α_{of} thermal diffusivity and ν_{of} kinematic viscosity.

We use Eq. (A20) up to $R_{aD} = 4.44 \times 10^8$, above the specified R_{aD} upper limit of 10^8. This is acceptable given that only relations for warm cylinders (i.e. those with outside wall temperature warmer than the adjacent air) are otherwise available and use of these yields similar values for h_{of}. For instance, use of relation (16b) in Tahavvor and Yaghoubi (2008), valid for warm cylinders and $R_{aD} > 10^8$, yields h_{of} values ranging from 3.9–5.4 $\mathrm{W\,m^{-2}\,K^{-1}}$ for Fig. A3 compared to 4.1–7.1 $\mathrm{W\,m^{-2}\,K^{-1}}$ using Eq. (A20). Differences between computed $T_{out} - T_{in}$ values were all $< 0.01\,°C$.

Similar to Eq. (A19):

$$h_{of} = \frac{Nu_{of}k_{of}}{D_o} \tag{A21}$$

Dimensionless parameters and other variables computed to find h_{if} and h_{of} are calculated respectively at the inside and outside film temperatures (T_{if} and T_{of}), taken to be:

$$T_{if} = \frac{T_3 + T_{ave}}{2} \tag{A22}$$

$$T_{of} = \frac{T_1 + T_2}{2} \tag{A23}$$

The intake warming model is solved iteratively from initial guesses for T_{out}, h_{if} and h_{of} with T_{out} updated each iteration as follows: $T_{out_{n+2}} = \frac{T_{out_n} + T_{out_{n+1}}}{2}$ where n is iteration number.

We adopt an upper limit for engine room air temperature of 50 °C and vary inlet temperature in 1 °C intervals between 0 and 30 °C. Pipe inside diameter is varied from around 6 to 37 cm corresponding to a range of standard outside diameters with wall thicknesses of common upper limit (Table A1).

Pipe inside diameters are dependent on engine horsepower and type and determined from volume flux requirements for engine cooling. Saur (1963) found these to vary between 4 and 20 inches (around 10 to 50 cm) on 12 US military vessels. Piip (1974) noted well thermometers were inserted into engine intakes to at least 25 cm depth, so inside diameters were likely at least double this. Tabata (1978) reports an engine intake pipe of 20 cm diameter on a Canadian research vessel. A typical inside diameter on a modern 100 000 t diesel tanker would be ∼ 25 cm. Intakes on steamships were likely larger still given that steam engines are closed cycle and so do not expel some of their waste heat through gaseous exhaust like diesel engines. Flow velocities are more consistent and fairly independent of pipe size, typically around 1–1.5 m s^{-1} with an upper limit of 3 m s^{-1}. To derive Fig. A3 we adopted a fixed pipe length of 20 m, above the upper end of inlet-thermometer distances reported in the literature (Table A2). Seawater specific heat capacity, thermal conductivity and dynamic viscosity were calculated using the Massachusetts Institute of Technology Thermophysical properties of seawater toolbox (http://web.mit.edu/seawater/), specifying a salinity of 35 psu.

References

Brooks, C. F.: Observing water-surface temperatures at sea, Mon. Weather Rev., 54, 241–253, doi:10.1175/1520-0493(1926)54<241:OWTAS>2.0.CO;2, 1926.

Delcroix, T., Alory, G., Diverres, D., Gouriou, Y., Jacquin, S., Maes, C., Morrow, R., Reverdin, G., Téchiné, P., Varillon, D., and the US IMAGO structure: Monitoring Sea Surface Salinity in the Global Ocean from Ships of Opportunity: the French SSS Observation Service, in: Proceedings of OceanObs'09: Sustained Ocean Observations and Information for Society (Annex), Venice, Italy, 21–25 September 2009, edited by: Hall, J., Harrison, D. E., and Stammer, D., ESA Publication WPP-306, doi:10.5270/OceanObs09, 2010.

Donlon, C. J., Minnett, P. J., Gentemann, C., Nightingale, T. J., Barton, I. J., Ward, B., and Murray, M. J.: Toward improved validation of satellite sea surface skin temperature measurements for climate research, J. Climate, 15, 353–369, doi:10.1175/1520-0442(2002)015<0353:TIVOSS>2.0.CO;2, 2002.

Donlon, C. J., Martin, M., Stark, J., Roberts-Jones, J., Fiedler, E., and Wimmer, W.: The operational sea surface temperature and sea ice analysis (OSTIA) system, Remote Sens. Environ., 116, 140–158, doi:10.1016/j.rse.2010.10.017, 2012.

Folland, C. K. and Parker, D. E.: Correction of instrumental biases in historical sea surface temperature data, Q. J. R. Meteorol. Soc., 121, 319–367, doi:10.1002/qj.49712152206, 1995.

Gnielinski, V.: New equations for heat and mass transfer in turbulent pipe and channel flow, Int. Chem. Eng., 16, 359–368, 1976.

Homayoni, H. and Yaghoubi, M.: Investigation of aiding flow for natural convection around a horizontal isothermal circular cylinder by finite volume, in: Proceedings of the 1st WSEAS International Conference on Finite differences – Finite Elements – Finite Volumes – Boundary Elements (F-and-B'08), Malta, September 11–13 2008, 79–83, 2008.

James, R. W. and Fox, P. T.: Comparative Sea-Surface Temperature Measurements, WMO, Geneva, Switzerland, 1972.

James, R. W. and Shank, M. K.: Effect of Variation of Intake Depths on Water Injection Temperatures, Marine Sciences Department, US Naval Oceanographic Office, Washington, DC, USA, 1964.

Kennedy, J. J., Rayner, N. A., Smith, R. O., Parker, D. E., and Saunby, M.: Reassessing biases and other uncertainties in sea surface temperature observations measured in situ since 1850: 1. measurement and sampling uncertainties, J. Geophys. Res., 116, D14103, doi:10.1029/2010JD015218, 2011a.

Kennedy, J. J., Rayner, N. A., Smith, R. O., Parker, D. E., and Saunby, M.: Reassessing biases and other uncertainties in sea surface temperature observations measured in situ since 1850: 2. Biases and homogenization, J. Geophys. Res., 116, D14104, doi:10.1029/2010JD015220, 2011b.

Kent, E. C., Woodruff, S. D., and Berry, D. I.: Metadata from WMO Publication No. 47 and an Assessment of Voluntary Observing Ship Observation Heights in ICOADS, J. Atmos. Oceanic Technol., 24, 214–234, doi:10.1175/JTECH1949.1, 2007.

Kent, E. C., Kennedy, J. J., Berry, D. I., and Smith, R. O.: Effects of instrumentation changes on sea surface temperature measured in situ, Climate Change, 1, 718–728, doi:10.1002/wcc.55, 2010.

Matthews, J. B. R.: Comparing Historical and Modern Sea Surface Temperature measurements methods in the Tropical Pacific, B.Sc. dissertation, University of East Anglia, Norwich, UK, 2009.

Matthews, J. B. R.: Comparing historical and modern methods of Sea Surface Temperature measurement – Part 1: Review of methods, field comparisons and dataset adjustments, Ocean Sci. Discuss., 9, 2951–2974, doi:10.5194/osd-9-2951-2012, 2012.

McCabe, W. L., Smith, J. C., and Harriott, P.: Unit Operations of Chemical Engineering, 6th edn., McGraw-Hill, New York, NY, USA, 2001.

Petit de la Villéon, L., Keeley, R., Gunn, J., Rutz, S., Gaillard, F., Reverdin, G., Goni, G., Delcroix, T., Carval, T., and the GOSUD contributing partners: GOSUD: Global Ocean Surface Underway Data Pilot Project, in: Proceedings of OceanObs'09: Sustained Ocean Observations and Information for Society (Annex), Venice, Italy, 21–25 September 2009, edited by: Hall, J., Harrison, D. E., and Stammer, D., ESA Publication WPP-306, doi:10.5270/OceanObs09, 2010.

Title Page

Abstract | Introduction

Conclusions | References

Tables | Figures

|◄ | ►|

◄ | ►

Back | Close

Full Screen / Esc

Printer-friendly Version

Interactive Discussion

Petukhov, B. S.: Heat transfer and friction in turbulent pipe flow with variable physical properties, Adv. Heat Transf., 6, 503–564, 1970.

Piip, A. T.: A Critical Description of the CSIRO Sea Surface Temperature and Salinity Sampling Program from Merchant Ships, Marine Laboratory, Cronulla, NSW, Australia, 1974.

Rayner, N. A., Parker, D. E., Horton, E. B., Folland, C. K., Alexander, L. V., Rowell, D. P., Kent, E. C., and Kaplan, A.: Global analyses of sea surface temperature, sea ice, and night marine air temperature since the late nineteenth century, J. Geophys. Res., 108, 4407, doi:10.1029/2002JD002670, 2003.

Rayner, N. A., Brohan, P., Parker, D. E., Folland, C. K., Kennedy, J. J., Vanicek, M., Ansell, T. J., and Tett, S. F. B.: Improved analyses of changes and uncertainties in sea surface temperature measured in situ since the mid-nineteenth century: the HadSST2 dataset, J. Climate, 19, 446–469, doi:10.1175/JCLI3637.1, 2006.

Saur, J. F. T.: A Study of the quality of sea water temperatures reported in logs of ships' weather observations, J. Appl. Meteor., 2, 417–425, doi:10.1175/1520-0450(1963)002<0417:ASOTQO>2.0.CO;2, 1963.

Siuda, A. N. S.: Final report for S.E.A. Cruise S217, Sea Education Association, Woods Hole, MA, 2008.

Smith, T. M. and Reynolds, R. W.: Bias corrections for historical sea surface temperatures based on marine air temperatures, J. Climate, 15, 73–87, doi:10.1175/1520-0442(2002)015<0073:BCFHSS>2.0.CO;2, 2002.

Smith, T. M. and Reynolds, R. W.: Improved extended reconstruction of SST (1854–1997), J. Climate, 17, 2466–2477, doi:10.1175/1520-0442(2004)017<2466:IEROS>2.0.CO;2, 2004.

Smith, T. M., Reynolds, R. W., Peterson, T. C., and Lawrimore, J.: Improvements to NOAA's historical merged land-ocean surface temperature analysis (1880–2006), J. Climate, 21, 2283–2296, doi:10.1175/2007JCLI2100.1, 2008.

Soloviev, A. and Lukas, R.: The Near-Surface Layer of the Ocean: Structure, Dynamics and Applications, Springer, Dordrecht, The Netherlands, 2006.

Tabata, S.: An examination of the quality of sea-surface temperatures and salinities observed recently in the Northeast Pacific Ocean, Pacific Marine Science Report 78-3, Institute of Ocean Sciences, Sidney, BC, Canada, 1978.

Tahavvor, A. R. and Yaghoubi, M.: Natural cooling of horizontal cylinder using Artificial Neural Network (ANN), Int. Commun. Heat Mass Transf., 35, 1196–1203, doi:10.1016/j.icheatmasstransfer.2008.05.009, 2008.

Field comparison of SST measurement methods

J. B. R. Matthews and J. B. Matthews

Title Page

Abstract	Introduction
Conclusions	References
Tables	Figures

|◄ | ►|

◄ | ►

Back | Close

Full Screen / Esc

Printer-friendly Version

Interactive Discussion

Thomas, B. R., Kent, E. C., and Swail, V. R.: Methods to homogenize wind speeds from ships and buoys, Int. J. Climatol., 25, 979–995, doi:10.1002/joc.1176, 2005.

Uwai, T. and Komura, K.: The Collection of Historical Ships' Data in Kobe Marine Observatory, in: Proceedings of the International COADS Workshop, Boulder, CO, USA, 13–15 January 1992, 1992.

Vecchi, G. A., Clement, A., and Soden, B. J.: Examining the Tropical Pacific's Response to Global Warming, Eos Trans. AGU, 89, 81–83, doi:10.1029/2008EO090002, 2008.

Wilkinson, C., Woodruff, S. D., Brohan, P., Claesson, S., Freeman, E., Koek, F., Lubker, S. J., Marzin, C., and Wheeler, D.: Recovery of logbooks and international marine data: the RE-CLAIM project, Int. J. Climatol., 31, 968–979, doi:10.1002/joc.2102, 2011.

Woodruff, S. D., Worley, S. J., Lubker, S. J., Ji, Z., Freeman, J. E., Berry, D. I., Brohan, P., Kent, E. C., Reynolds, R. W., Smith, S. R., and Wilkinson, C.: ICOADS Release 2.5: extensions and enhancements to the surface marine meteorological archive, Int. J. Climatol., 31, 951–967, doi:10.1002/joc.2103, 2011.

Field comparison of SST measurement methods

J. B. R. Matthews and J. B. Matthews

Title Page

Abstract | Introduction

Conclusions | References

Tables | Figures

|◄ | ►|

◄ | ►

Back | Close

Full Screen / Esc

Printer-friendly Version

Interactive Discussion

Table 1. Average upper 3 m temperature differences and eastward surface velocities in various current regimes encountered along the cruise transect. The regimes exhibit distinct differences in surface current velocity and/or direction. Four currents were recognised along the transect: the South Equatorial Current (SEC), the South Equatorial Countercurrent (SECC), the North Equatorial Countercurrrent (NECC) and the North Equatorial Current (NEC). Adjectives in regime names describe relative current strength in sub-branches of these currents.

Regime	Approximate latitudinal range ($°N$)	Eastward surface current velocity (cms^{-1})	Composite bucket SST minus 3 m temperature ($°C$)		
			All	Day	Night
SEC Weak	−17.5 to −12.4	−5.5 ± 11.1	0.4 ± 0.2	0.5 ± 0.1	0.4 ± 0.1
SEC Moderate	−12.4 to −10.3	−10.6 ± 14.4	0.4 ± 0.2	0.5 ± 0.2	0.3 ± 0.1
SECC	−10.3 to −8.8	4.0 ± 9.1	0.4 ± 0.2	0.6 ± 0.3	0.3 ± 0.1
SEC Strong	−8.8 to −2.5	−19.7 ± 21.2	0.3 ± 0.1	0.4 ± 0.2	0.3 ± 0.1
Cold tongue (NECC)	−2.5 to 1.4	55.1 ± 25.6	0.3 ± 0.1	0.4 ± 0.1	0.3 ± 0.1
NECC (outside cold tongue)	1.4 to 5.7	29.8 ± 8.3	0.3 ± 0.1	0.4 ± 0.1	0.3 ± 0.1
NEC Strong	5.7 to 11.0	−23.3 ± 14.3			
NEC Weak	11.2 to 19.0	−8.3 ± 10.4			

Table A1. Intake pipe specifications used to generate Figs. A3 and A4.

Outside diameter (cm)	Wall thickness (cm)	Schedule	Inside diameter (cm)	Nominal bore (inches)
8.89	1.52	XXS	5.85	3
11.43	1.71	XXS	8.01	4
14.13	1.90	XXS	10.33	5
16.83	2.20	XXS	12.43	6
21.91	2.30	160	17.31	8
27.30	2.54	XXS	22.22	10
32.39	3.33	160	25.73	12
35.56	3.57	160	28.42	14
40.64	4.05	160	32.54	16
45.72	4.52	160	36.68	18

Table A2. Inlet-thermometer pipe lengths reported in the literature.

Reference	Pipe length from inlet to thermometer
Saur (1963)	Few feet to 25 feet
James and Fox (1972)	0–9 m
Piip (1974)	3–15 m
Tabata (1978)	~ 1 m

Table A3. Fixed parameters of our seawater intake warming model including their value(s) for Figs. A3 and A4.

Model parameter	Symbol	Value(s)	Unit
Pipe inside diameter	D_i	0.0585–0.3668	m
Pipe outside diameter	D_o	0.0889–0.4572	m
Pipe wall thickness	Δx_w	0.0152–0.0452	m
Surface area of inside wall	A_i	3.7–23.0	m^2
Surface area of outside wall	A_o	5.6–28.7	m^2
Log-mean wall surface area	A_{lm}	4.6–25.8	m^2
Inside cross-sectional area	A_c	2.688×10^{-3}–1.057×10^{-1}	m^2
Thermal conductivity of pipe wall (unlagged steel)	k_w	45	$W\,m^{-1}\,K^{-1}$
Flow velocity	u	1	$m\,s^{-1}$
Volumetric flow rate	$\dot{v}$	2.688×10^{-3}–1.057×10^{-1} (2.7–$105.7\,l\,s^{-1}$)	$m^3\,s^{-1}$
Engine room air temperature	T_1	50	°C
Seawater temperature at inlet	T_{in}	0–30	°C
Seawater salinity	S	35	psu
Acceleration due to gravity	g	9.81	$m\,s^{-2}$

Table A4. Variables computed by the seawater intake warming model including their calculated range in Fig. A3.

Model variable	Symbol	Computed range	Unit
Outside wall temperature	T_2	0.35–30.13	°C
Inside wall temperature	T_3	0.16–30.07	°C
Inside film temperature	T_{if}	0.08–30.05	°C
Outside film temperature	T_{of}	25.18–40.06	°C
Seawater temperature after pipe length L	T_{out}	0.02–30.05	°C
Bulk seawater temperature	T_{ave}	0.01–30.03	°C
Log-mean temperature difference across the pipe wall	ΔT_{lm}	19.97–49.99	°C
Seawater temperature difference between inlet and thermometer	ΔT	0.01–0.18	°C
Overall inside heat transfer coefficient	U_i	5.1–10.7	$W\,m^2\,K^{-1}$
Heat transfer rate	q	596.6–7779.1	W
Seawater specific heat capacity	c_p	3991.1–4003.1	$J\,kg^{-1}\,K^{-1}$
Seawater density	ρ	1021.7–1028.1	$kg\,m^{-3}$
Mass flow rate	$\dot{m}$	2.7–108.6	$kg\,s^{-1}$
Seawater thermal conductivity (inside film)	k_{if}	0.57–0.62	$W\,m^{-1}\,K^{-1}$
Air thermal conductivity (outside film)	k_{of}	0.03	$W\,m^{-1}\,K^{-1}$
Reynolds number (inside film)	Re_{if}	3.18×10^4–4.36×10^5	dimensionless
Prandtl number (inside film)	Pr_{if}	5.59–13.31	dimensionless
Seawater dynamic viscosity (inside film)	μ_{if}	8.60×10^{-4}–1.90×10^{-3}	$kg\,m^{-1}\,s^{-1}$
Friction factor	f	1.35×10^{-2}–2.33×10^{-2}	dimensionless
Air thermal diffusivity (outside film)	α_{of}	2.23×10^{-5}–2.45×10^{-5}	$m^2\,s^{-1}$
Air thermal expansion coefficient (outside film)	β_{of}	3.19×10^{-3}–3.35×10^{-3}	K^{-1}
Air kinematic viscosity (outside film)	v_{of}	1.57×10^{-5}–1.72×10^{-5}	$m^2\,s^{-1}$
Rayleigh number for characteristic length D_o	Ra_D	1.04×10^6–4.44×10^8	dimensionless
Nusselt number (inside film)	Nu_{if}	286.1–1929.7	dimensionless
Nusselt number (outside film)	Nu_{of}	17.5–95.5	dimensionless
Convective heat transfer coefficient (inside film)	h_{if}	2221.6–4178.6	$W\,m^2\,K^{-1}$
Convective heat transfer coefficient (outside film)	h_{of}	4.1–7.1	$W\,m^2\,K^{-1}$
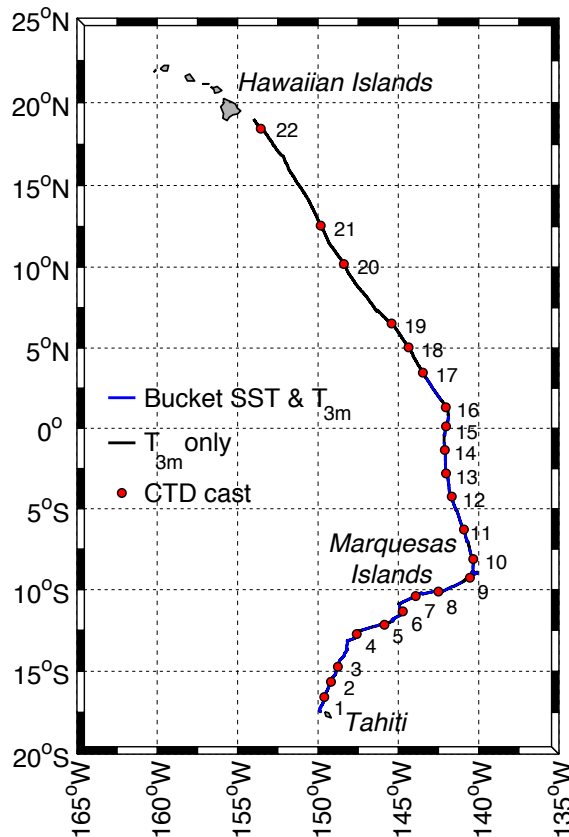
Fig. 1. Map of the cruise transect across the Central Tropical Pacific. The blue line denotes the portion of the transect where both bucket and 3 m thermosalinograph temperatures were observed. The black line denotes the subsequent portion where bucket temperatures were not taken. Locations of CTD casts are marked by red dots.

Fig. 2. From left to right; the wood, canvas and rubber buckets used in our field comparison. Note that the wooden bucket was sealed with white caulk along the inner seams and reinforced around the outside by two stainless steel bands. The rubber bucket is of both plastic and rubber construction with a black rubber protective layer around the base.

Fig. 3. Histograms of differences between near-simultaneous sea surface temperatures obtained with **(a)** wood and canvas buckets, **(b)** rubber and canvas buckets and **(c)** rubber and wood buckets. A value of 0.7 °C is excluded from **(b)**, hence this subplot has one fewer total number of stations than **(a)** and **(c)**.
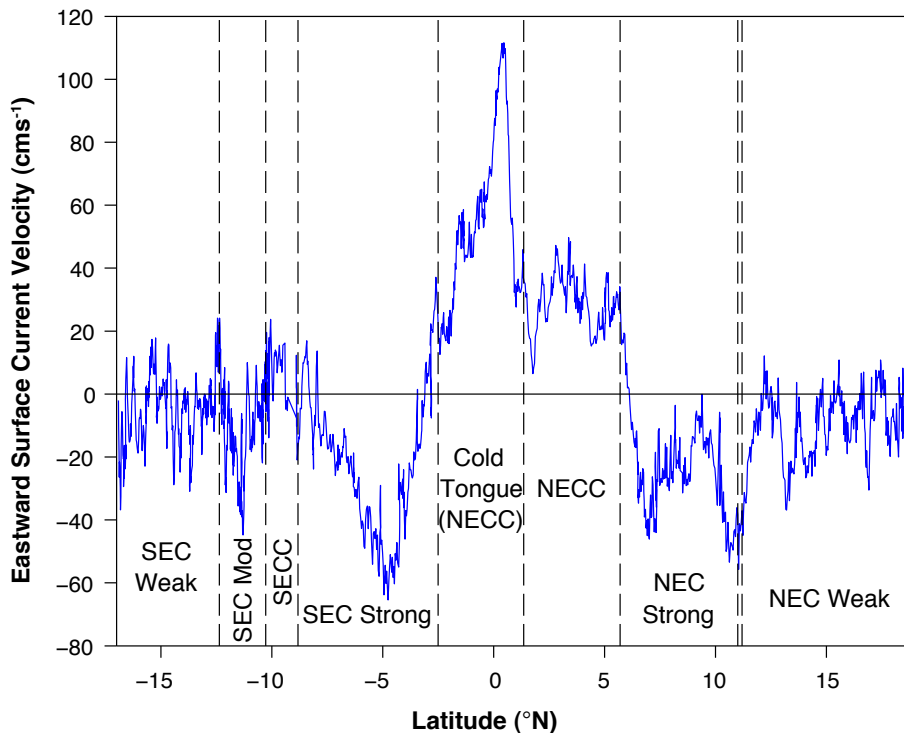
Fig. 4. Eastward surface current velocity (∼ 19 m depth) along the cruise transect between ∼ 17° S and 19° N as measured by Acoustic Doppler Current Profiler. Dashed lines and associated text labels indicate surface current regimes identified in Table 1. "Mod" means moderate.
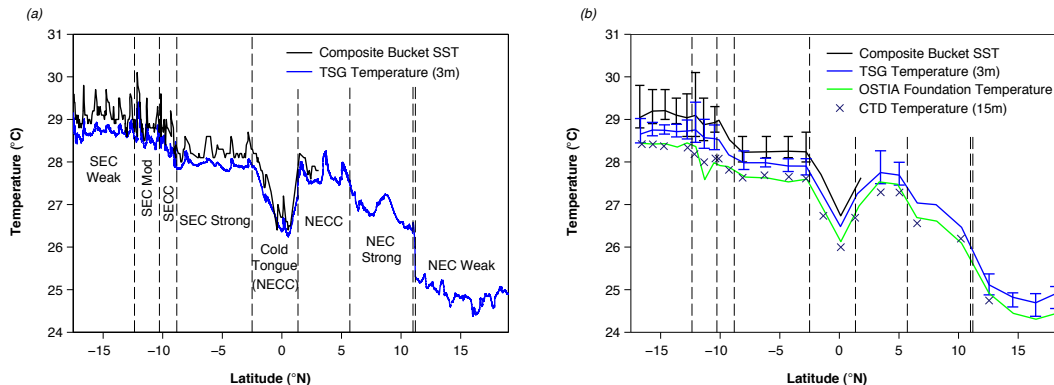
Fig. 5. Meridional temperature structure of the surface and near-surface along the cruise transect: **(a)** Composite bucket SST and 3 m thermosalinograph temperature; **(b)** daily-average composite bucket SST, 3 m temperature, OSTIA foundation temperature and 15 m CTD temperature. The maximum and minimum values of composite bucket SST and 3 m temperature on each local day are denoted by the upper and lower bars (not plotted in surface regimes with strong meridional temperature gradients). Surface regimes are demarcated as in Fig. 4.
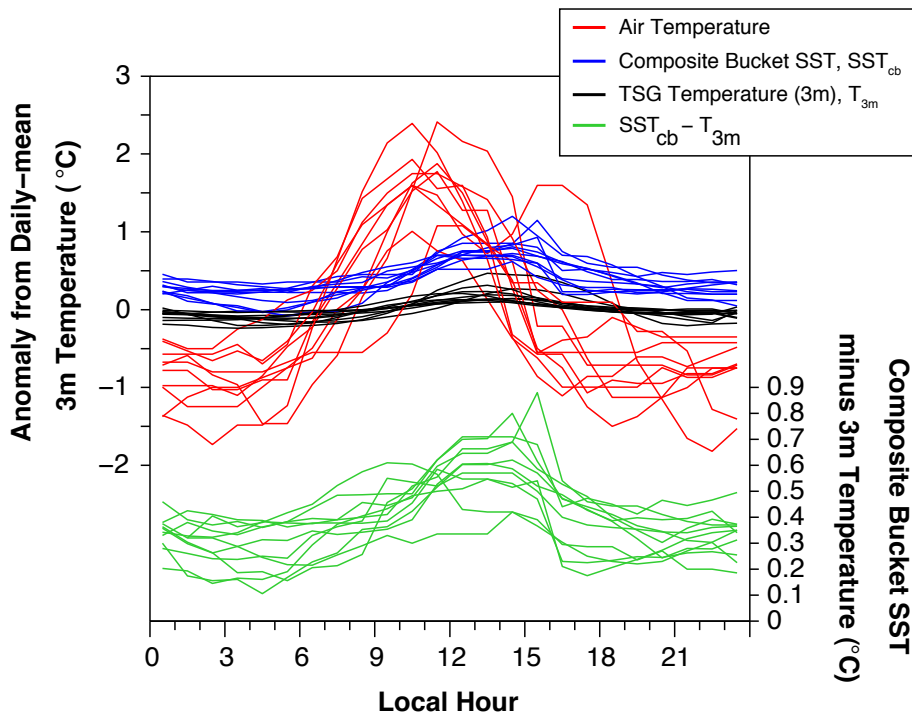
Fig. 6. Diurnal cycles within the weak, moderate and strong branches of the South Equatorial Current from three-hour moving averages. Air temperature, composite bucket SST and 3 m thermosalinograph temperature are plotted on the left-hand axis and expressed as anomalies from daily-mean 3 m temperature for the respective local day. Temperature difference across the upper 3 m is plotted on the right-hand axis.

Title Page

Abstract | Introduction

Conclusions | References

Tables | Figures

◄ | ►

◄ | ►

Back | Close

Full Screen / Esc

Printer-friendly Version

Interactive Discussion
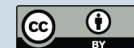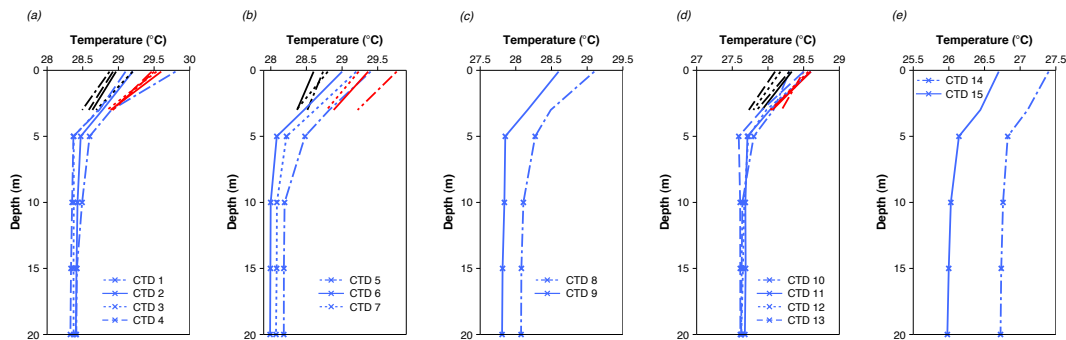
Fig. 7. Temperature structure of the upper 20 m in various current regimes along the cruise transect: **(a)** the weak and **(b)** moderate branches of the South Equatorial Current (SEC), **(c)** the South Equatorial Countercurrrent (SECC), **(d)** the strong branch of the SEC and **(e)** the equatorial cold tongue. The blue lines are temperature profiles corresponding to individual CTD casts. Temperatures at 5, 10, 15 and 20 m are from CTD (indicated by the crosses) while those at 0.1 and 3 m are from composite bucket SST and thermosalinograph, respectively. The composite bucket SST values were obtained within 3 h and 15 km of each respective CTD cast. All casts were taken between 09:00 a.m. and noon local time, except CTD-1 which was taken around 15:30–16:00 LT. Cast numbers correspond to those on Fig. 1. The red and black lines characterize the daily extremes of the upper 3 m temperature profile on the local day of the corresponding CTD cast. They are respectively defined from maximum and minimum 3-h average 3 m temperatures, and corresponding 3-h average composite bucket temperatures. They are not plotted in the panels for the SECC and cold tongue, where diurnal cycles were masked by transit through strong meridional temperature gradients.

(a)

(b)
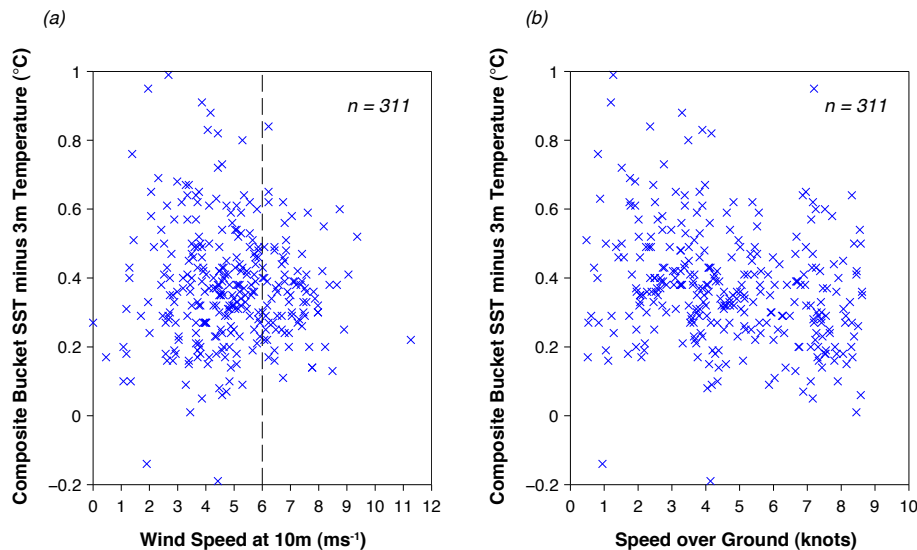
Fig. 8. Scatter plots comparing upper 3 m temperature differences with **(a)** true wind speed at 10 m and **(b)** speed over ground of the *Seamans*. The vertical dashed line on **(a)** denotes a wind speed of 6 m s^{-1}. General thinking holds that the near-surface should be near-isothermal at higher wind speeds.
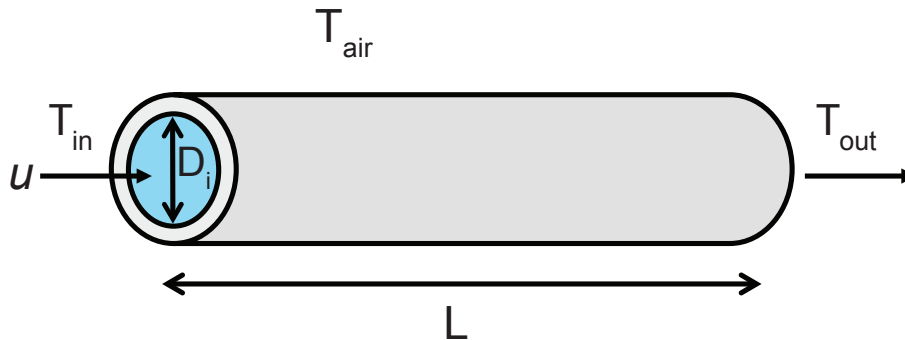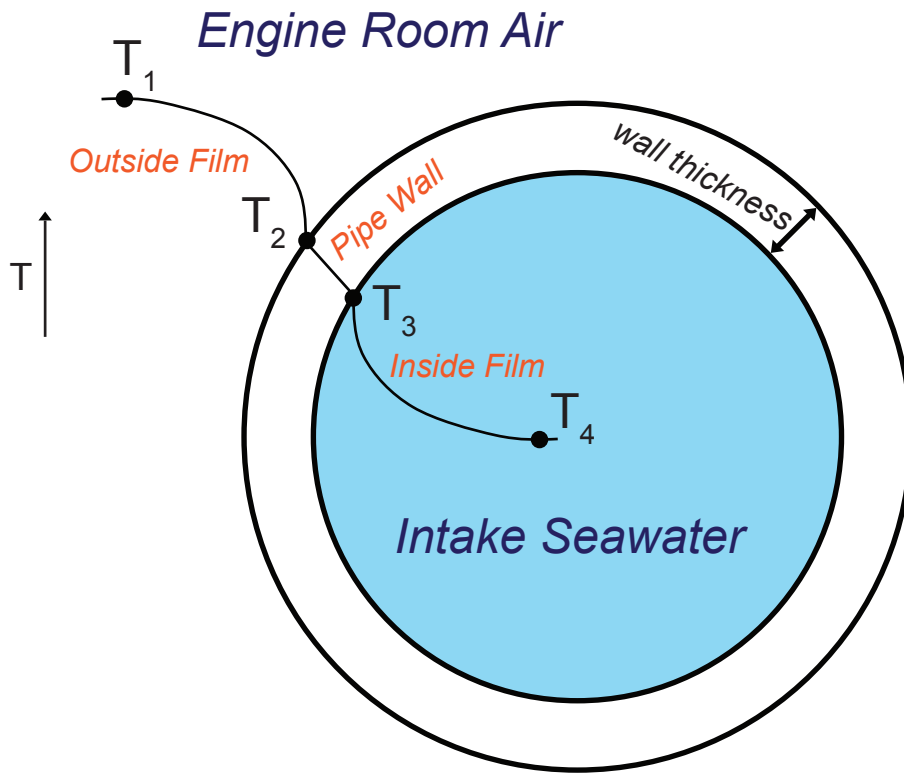
Fig. A1. Schematic of our model for warming of intake seawater by engine room air at temperature T_{air}. The seawater is flowing at velocity u in a pipe of inside diameter D_i. The initial seawater temperature is T_{in} and the temperature after pipe length L is T_{out}.

Fig. A2. Cross-section through the modelled intake pipe. An illustrative temperature profile is shown by the solid black lines connecting temperatures T_1, T_2, T_3 and T_4 with engine room air temperature, T_1, being the warmest.
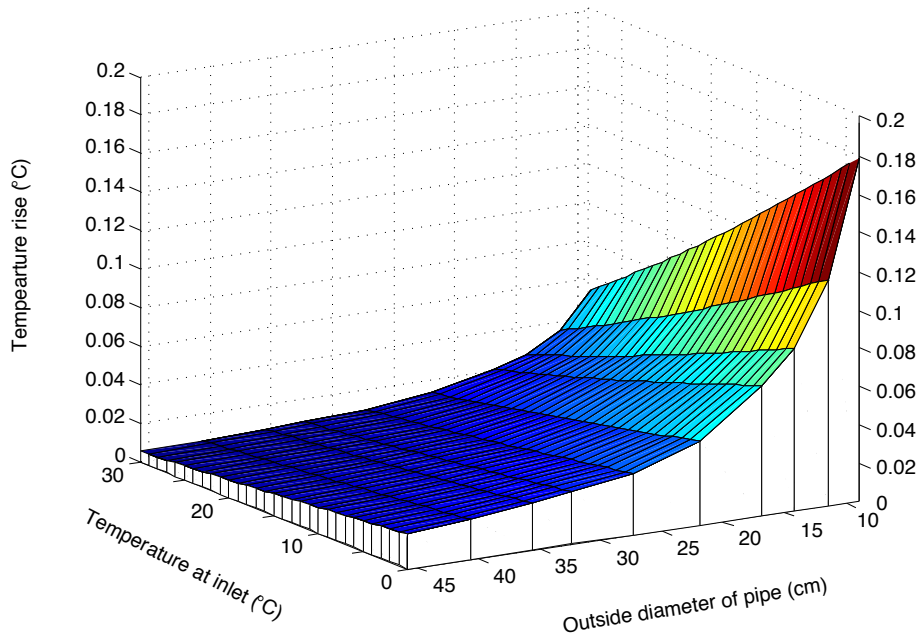
Fig. A3. Calculated warming of seawater along an intake pipe of length 20 m for variable outside diameter and inlet temperature. Engine room air temperature was set to 50 °C and flow velocity to $1\,\mathrm{m\,s}^{-1}$.

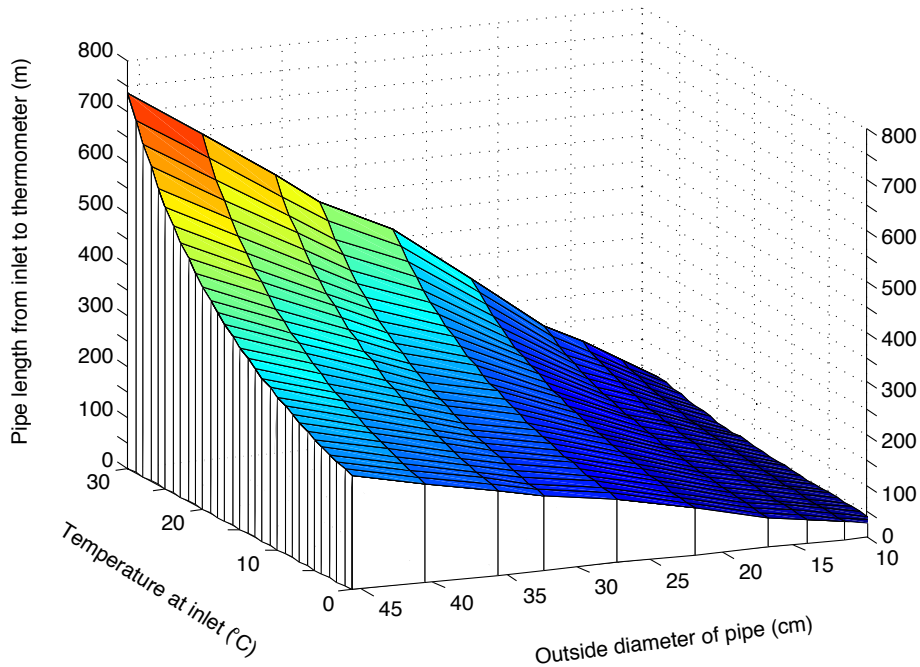**Fig. A4.** Pipe length required for intake seawater to warm by 0.2 °C given an engine room air temperature of 50 °C and flow velocity of $1\,\mathrm{m\,s^{-1}}$.

OSD

9, 2975–3019, 2012

Field comparison of SST measurement methods

J. B. R. Matthews and J. B. Matthews

Title Page

Abstract   Introduction

Conclusions   References

Tables   Figures

◄◄   ►►

◄   ►

Back   Close

Full Screen / Esc

Printer-friendly Version

Interactive Discussion